LAUNCH WINDOW ANALYSIS FOR THE MAGNETOSPHERIC MULTISCALE MISSION

Trevor Williams[1]

The NASA Magnetospheric Multiscale (MMS) mission will fly four spinning spacecraft in formation in highly elliptical orbits to study the magnetosphere of the Earth. This paper describes the development of an MMS launch window tool that uses the orbit-averaged Variation of Parameter equations as the basis for a semi-analytic quantification of the dominant oblateness and lunisolar perturbation effects on the MMS orbit. This approach, coupled with a geometric interpretation of all of the MMS science and engineering constraints, allows a scan of 180^2 = 32,400 different (RAAN, AOP) pairs to be carried out for a specified launch day in less than 10 s on a typical modern laptop. The resulting plot indicates the regions in (RAAN, AOP) space where each constraint is satisfied or violated: their intersection gives, in an easily interpreted graphical manner, the final solution space for the day considered. This tool, SWM76, is now used to provide launch conditions to the full fidelity (but far slower) MMS simulation code: very good agreement has been observed between the two methods.

INTRODUCTION

The NASA Magnetospheric Multiscale (MMS) mission [1] will fly four spinning spacecraft in formation in highly elliptical orbits to study the magnetosphere of the Earth. A key objective is to perform *in situ* data collection during the extremely energetic magnetic reconnection events. These events are expected to occur on the dayside of the Earth, broadly in the vicinity of the bowshock that is produced by the impinging solar wind (at distances of around 10-12 Earth radii (R_E) from the center of the Earth), and on the nightside, at radii of around 20-25 R_E, in the magnetotail. In order to carry out these measurements the spacecraft will fly in formations that take up broadly tetrahedral forms, of various sizes, in the region surrounding the apogee of their highly eccentric orbits, at which science data is collected. In addition, the MMS orbits must be carefully aligned with respect to the Earth-Sun line and have the appropriate apogee radii for the region of the magnetosphere that is currently being studied. Launch is planned for late 2014 with the spacecraft first carrying out science on the dayside in orbits with apogee radius 12 R_E and perigee radius 1.2 R_E, then increasing apogee radius to 25 R_E in order to study the magnetotail.

The MMS orbit must satisfy many constraints, arising from both scientific and engineering considerations. For instance, if the spacecraft were to encounter eclipses of excessive duration, power and/or thermal problems could result. In addition, since the satellites are spinners, the large apogee-raising burns (which occur over an long arc in the orbit plane around perigee, as a result of the low MMS thrust) will be shown to consume excessive fuel, as a result of Triangle Inequality losses, if the inertially fixed spin axis makes too large an angle to the orbit normal. Science requirements include that the apogee vector at the start of science collection should be close to dusk, the solar latitude of apogee during the dayside magnetosphere passes should be small, and sufficient time be spent in the neutral sheet region of the magnetotail during the nightside passage that the probability of observing enough magnetic reconnection events is high.

The initial MMS orbit has specified apogee and perigee radii and inclination. The problem of determining a launch window on a specified day of the year therefore amounts to specifying acceptable launch values

[1] Aerospace Engineer, Navigation and Mission Design Branch, NASA Goddard Space Flight Center, Greenbelt, MD 20771. Associate Fellow, AIAA. Phone: (301)286-8204. Email: Trevor.W.Williams@nasa.gov

for the Right Ascension of the Ascending Node (RAAN) and Argument of Perigee (AOP). Mapping the science and engineering constraints, most of which apply at points months after launch, to the initial RAAN and AOP is made much more complicated by the fact that the MMS orbit is low enough at perigee to be significantly affected by the oblateness of the Earth, and high enough at apogee to be significantly perturbed by lunar and solar effects. A full mission simulation based on traditional point-by-point orbital propagation takes far too long to allow many possible (RAAN, AOP) pairs to be scanned over, as is desired for a launch window analyzer.

This paper describes the development of an MMS launch window tool, termed SWM76, which uses the Variation of Parameter (VOP) equations [5] as the basis for a semi-analytic quantification of the dominant oblateness and lunisolar perturbation effects on the MMS orbit. Instead of applying a full force model over successive, necessarily short, time steps, this approach averages the effects of the relatively small perturbations over a complete MMS orbit and then applies these lunisolar and oblateness corrections to the orbital elements. The result is an accurate approximation to the perturbed MMS orbit, but obtained with much greater computational efficiency. In fact, this approach, coupled with an interpretation of the MMS science and engineering constraints in terms of *geometry proxies* (e.g. solar latitude used as a proxy for eclipse durations), allows a scan through all possible RAAN and AOP values (0-360 deg) for a given launch date, in 2 deg steps, to be carried out in less than 10 s on a typical modern laptop. By comparison, evaluating a single one of these $180^2 = 32{,}400$ (RAAN, AOP) pairs using the much more detailed MMS End-to-End (ETE) simulation code, which uses full force model point-by-point propagation, and includes formation maneuvers with navigation and execution errors, etc., takes 6-8 hr. SWM76 has therefore proved to be a valuable adjunct to the ETE code, allowing good launch RAAN and AOP values to be generated for use by the latter. It should be noted that good agreement has been observed between the predictions of SWM76 and the results generated by the ETE code.

In addition, the results produced by SWM76 are in graphical form: they show the regions in the (RAAN, AOP)-plane over which each of the MMS orbital constraints is satisfied. The launch window (if any exists) for this date is then the intersection of these regions. This graphical output form has proved to be very useful for providing insight into which constraints are most onerous, and so could be most profitable to relax, allowing launches to be possible on a wider range of dates. SWM76 also provides additional outputs, such as the minimum perigee altitude reached during the mission: this is a result of lunisolar perturbations, and is a strong function of RAAN, AOP and launch date. Knowledge of the minimum perigee altitude is useful for predicting the amount of fuel that MMS will require for orbit maintenance: this is an important question, given the extensive maneuvering that MMS must carry out.

The paper is organized as follows. The requirements that must be satisfied by the MMS orbit are first outlined, followed by the development of geometry proxies (in the main angles) that can be used to evaluate these. The properties of the key orbital perturbations that act on the spacecraft (Earth oblateness and lunisolar effects) are then described, followed by the orbit-averaged VOP approach for efficient determination of their effects on the MMS orbit. This is then followed by a discussion of techniques used to improve the computational efficiency of the SWM76 Matlab code, with finally a discussion of results obtained using this program.

MMS LAUNCH WINDOW DETERMINATION PROBLEM

The MMS spacecraft will be launched due East from Kennedy Space Center on an Atlas 5 launch vehicle. Initial injection will be into a circular parking orbit of altitude 240 km and inclination 28.5 deg. After an appropriate coast period, the Centaur upper stage will be reignited to place the spacecraft on an orbit with unchanged perigee altitude and inclination, but with apogee radius 12 R_E. A series of five maneuvers by the spacecraft over the first two weeks of the mission will then be used to raise perigee radius to 1.2 R_E, corresponding to an altitude of around 1,276 km.

The launch window problem can be stated as that of selecting values for the RAAN, Ω_0, and AOP, ω_0, for the MMS orbit such that the various MMS orbital mission constraints are satisfied. Some of these

requirements arise from engineering considerations, while others are defined to set the satellites up to collect the desired magnetospheric science. Note that selecting RAAN amounts to fixing the desired time of Atlas launch; selecting AOP corresponds to selecting the coast time between the initial parking orbit injection and the second Centaur burn to place the spacecraft on the highly eccentric MMS orbit.

The baseline MMS mission orbital requirements can be summarized as follows, in the order in which they arise during the mission (see Fig. 1 for a schematic representation of the mission).

Early mission eclipses
No eclipse of duration (defined as that of umbra plus half of penumbra) 1 hr or greater shall occur during the first 14 days of the mission.

Apogee solar longitude at Phase 1 start
In order to collect the desired science data, MMS must be able to run through a specified set of formation sizes at specified locations relative to the Sun. A consequence is that apogee at the start of Phase 1 must lie near dusk. This is the start of science collection, and follows the checkout and commissioning activities of the 120-day Phase 0. This solar longitude constraint is commonly described in terms of *Geocentric Solar Ecliptic* (*GSE) time* (described in more detail later) with this defined in the ecliptic plane as noted in Fig. 1: 0/24 hr corresponds to the down-Sun direction, 6 hr is 90 deg later, at dawn, 12 hr corresponds to directly up-Sun, and 18 hr lies at dusk. The baseline MMS requirement is that apogee, when projected onto the ecliptic plane, lie in the range 17-19 hr GSE.

Apogee solar latitude at Phases 1a, 1b
Dayside science collection is to occur in the region between Sun and Earth where magnetic reconnection is thought to occur. MMS has two dayside science passes: Phase 1a, which occurs roughly 7 months after launch, and Phase 1b, which takes place about one year after this. In order for the formation to be in position to detect reconnection events, it is desired that apogee not be too far out of the ecliptic during these passes. Specifically, the requirement is that the solar latitude of apogee lies in the range ±20 deg throughout Phase 1a, and ±25 deg during Phase 2b.

Apogee-raising fuel usage
The maneuvers that are used during Phase 2a to raise apogee from 12 R_E to 25 R_E consume a large fraction of the total MMS fuel capacity that, under the most favorable circumstances, use around 170 kg out of a total of 410 kg. The specific fuel usage depends on the orbit orientation in a way that will be discussed below. Because a majority of the total fuel onboard the spacecraft at launch is consumed for perigee-raising, apogee-raising, and formation maintenance and resize maneuvers, orbit geometries that lead to increased apogee-raising fuel usage are to be avoided.

Eclipse duration, Phase 2b
No eclipse of duration (defined as that of umbra plus half of penumbra) 3.85 hr or greater shall occur during at any point during the mission. In reality, eclipses of this duration typically only occur in the vicinity of apogee on the Phase 2b orbit when the satellites travel at their slowest speed (around 0.5 km/s). Consequently, this constraint is actually on eclipse durations in Phase 2b.

Neutral sheet dwell time
In order to be in position to be able to observe magnetic reconnection events in the magnetotail on the nightside of the Earth, the spacecraft must spend at least 100 hr flying within 0.5 R_E of the Fairfield model [2] of the *neutral sheet* (i.e. the surface that separates the northern and southern lobes) of the magnetotail. Note that this model is a simplified, averaged model based on extensive early satellite observations of the magnetosphere. In reality, the neutral sheet location depends on solar wind strength and direction, neither of which is known for the MMS mission timeframe at this point. The Fairfield model is therefore used as guideline. If MMS spends sufficient time in its vicinity, it is likely that the formation will be in position to observe a set of reconnection events.

A significant difficulty in evaluating these constraints is that many of them apply some considerable time after launch: commissioning takes 4 months, followed by a science mission that is roughly 2 years in duration. Over this interval the orbit is affected strongly by both the oblateness (i.e. the J_2 term in the gravity model) of the Earth (because the MMS perigee is relatively low); and it is also significantly affected by the gravitational attraction of both Sun and Moon (because the MMS apogee is high, particularly during Phase 2b). Consequently, a large part of the effort involved in carrying out an MMS launch window analysis is evaluating the J_2 and lunisolar effects on the orbit, so as to be able to map condition at any specified point on interest in the mission (e.g. Phase 2a, for apogee-raising) back to the initial launch conditions. This then allows a determination to be made of which launch RAAN and AOP lead to moderate apogee-raising fuel consumption, etc.

One further consideration is that the MMS perigee altitude is not allowed to go below 800 km. Lunisolar perturbations can cause perigee to dip below this threshold: this then triggers a pair of reboost maneuvers that typically consume as much as 30 kg of fuel. As this is a significant amount of fuel, it is of considerable interest to know how many reboosts are likely to be required for any given launch conditions.

GEOMETRY PROXIES FOR ORBIT CONSTRAINTS

The traditional approach to evaluating whether given values for the launch RAAN and AOP satisfy the orbit design constraints would be to do a detailed, point-by-point orbit propagation (with relatively short time steps, in order to give sufficient accuracy), and then directly check the resulting eclipse durations, neutral sheet dwell time, etc. to see if they satisfy the requirements. However, this type of method is computationally slow, and therefore poorly suited to evaluation of a wide set of launch conditions, as is required to investigate how the MMS launch window varies over the course of the year. It will be shown later in the paper how orbit-averaging of the VOP equations can be used to overcome the need for point-by-point propagation, which results in speeding up computation by two to three orders of magnitude.

A second key component to this method is then to determine eclipse durations etc. not by direct testing, but by evaluation of some *geometry proxy*, typically an angle (apart from for the early mission eclipse case), that is closely related to the quantity in question and so can be used to predict its value. Since the VOP equations are based on the orbital elements, the goal is to derive proxies that are readily computed from the elements and have good predictive qualities. The derivation of such quantities for the various MMS orbit design requirements will now be outlined. Several coordinate systems that will be needed for this work are as follows.

Earth-Centered Inertial (ECI) frame

- x_{ECI} : in the equatorial frame, directed from the center of the Earth to the center of the Sun on the vernal equinox;
- y_{ECI} : in the equatorial frame, 90 deg ahead of x_{ECI} in the direction of the orbital motion of the Earth;
- z_{ECI} : along the spin axis of the Earth.

In what follows, all vectors, when given in component form, will be expressed in terms of the ECI frame.

Geocentric Solar Ecliptic (GSE) frame

- x_{GSE} : in the ecliptic frame, directed from the center of the Earth to the center of the Sun;
- y_{GSE} : in the ecliptic plane, directed towards dusk;
- z_{GSE} : along the ecliptic normal.

The GSE frame therefore rotates at the rate of one counter-clockwise (as viewed from above) cycle per year. Note that Fig. 1 is shown in the GSE frame: the Sun (i.e. the $+x_{GSE}$-axis) is always to the left, and dusk (i.e. the $+y_{GSE}$-axis) directed down. The (roughly) inertially fixed MMS orbit therefore appears to complete (approximately) one clockwise rotation per year.

The GSE frame leads to the definition of *GSE time* as a measure of azimuth in the ecliptic: 0/24 hr is directed away from the Sun (i.e. local midnight; along the $-x_{GSE}$-axis), 6 hr is towards dawn (along the $-y_{GSE}$-axis), 12 hr towards noon ($+x_{GSE}$), and 18 hr towards dusk ($+y_{GSE}$).

Geocentric Solar Magnetospheric (GSM) frame

x_{GSM}: equal to x_{GSE};

y_{GSM}: perpendicular to both the x_{GSM} and magnetic dipole axes of the Earth;

z_{GSM}: completes the right-handed triad (note that positive z_{GSM} is directed broadly North).

The (x_{GSM}, z_{GSM})-plane therefore always contains the Earth dipole axis. The GSM and GSE frames differ only in a diurnal rotation of GSM about the *x*-axis: this is caused by the rocking of the dipole of the Earth, which results from its misalignment of roughly 11 deg from the spin axis of the Earth.

The geometry proxies used for MMS launch window analysis are the following.

Early mission eclipses

Eclipse durations can be quantified in terms of the orthogonal projection of the down-Sun unit vector onto the orbit plane: this is given as

$$\mathbf{x}_d = -\left[\hat{\mathbf{x}}_{GSE} - (\hat{\mathbf{x}}_{GSE}^T \hat{\mathbf{h}})\hat{\mathbf{h}}\right], \tag{1}$$

where $\hat{\mathbf{h}}$ is the orbit normal unit vector,

$$\hat{\mathbf{h}} = \begin{pmatrix} \sin\Omega\sin i \\ -\cos\Omega\sin i \\ \cos i \end{pmatrix}, \tag{2}$$

and the unit vectors defining the GSE frame, expressed in the geocentric inertial frame [5], are given as

$$\hat{\mathbf{x}}_{GSE} = \begin{pmatrix} \cos\psi \\ \sin\psi\cos\varepsilon \\ \sin\psi\sin\varepsilon \end{pmatrix}, \quad \hat{\mathbf{y}}_{GSE} = \begin{pmatrix} -\sin\psi \\ \cos\psi\cos\varepsilon \\ \cos\psi\sin\varepsilon \end{pmatrix}, \quad \hat{\mathbf{z}}_{GSE} = \begin{pmatrix} 0 \\ -\sin\varepsilon \\ \cos\varepsilon \end{pmatrix}; \tag{3}$$

y is the solar longitude, i.e. the inertial direction of the Earth-Sun line as a function of day of year, and ε the obliquity of the ecliptic (23.4 deg).

Normalizing the down-Sun projected vector defines the components

$$\hat{\mathbf{x}}_d = \mathbf{x}_d / \|\mathbf{x}_d\|_2 \equiv \begin{pmatrix} X \\ Y \\ Z \end{pmatrix}. \tag{4}$$

It can then be shown that the argument of latitude of the down-Sun line in the orbit plane, $u_d = \omega + \nu_d$, is given from the relations

$$\sin u_d = Z/\sin i \tag{5}$$

and

$$\cos u_d = \begin{cases} \left[X + Z\sin\Omega\cot i\right]/\cos\Omega, \\ \left[Y - Z\cos\Omega\cot i\right]/\sin\Omega. \end{cases} \tag{6}$$

Note: in order to avoid the possibility of singularities, the (theoretically) equivalent form for $\cos u_d$ with the largest denominator magnitude should be used.

For a given AOP, knowledge of the down-Sun argument of latitude allows the corresponding true anomaly to be readily found as $\nu_d = u_d - \omega$. It can then be shown that the time that the satellite will spend in eclipse (umbra plus half penumbra) is approximately given as

$$T_{ecl} = \frac{2\sqrt{R_E^3}}{(1+e\cos\nu_d)}\sqrt{\left(\frac{\tilde{p}}{\mu_{Earth}}\right)\left\{1-\left[\frac{\tilde{p}\left(\hat{\mathbf{h}}^T\hat{\mathbf{x}}_{GSE}\right)}{(1+e\cos\nu_d)}\right]^2\right\}}, \tag{7}$$

where $\tilde{p} \equiv p/R_E$. Note that, if the term in the square root is negative (so giving an imaginary result) or zero, no eclipse exists.

Apogee solar longitude (i.e. GSE time) at Phase 1 start

The unit vector directed from the center of the Earth to MMS apogee is given as

$$\hat{\mathbf{r}}_a = -\hat{\mathbf{e}} = \begin{pmatrix} -\cos\omega\cos\Omega + \sin\omega\sin\Omega\cos i \\ -\cos\omega\sin\Omega - \sin\omega\cos\Omega\cos i \\ -\sin\omega\sin i \end{pmatrix}. \tag{8}$$

The projection of this vector onto the ecliptic plane,

$$\mathbf{r}_{a\_xy} = \hat{\mathbf{r}}_a - \left(\hat{\mathbf{r}}_a^T\hat{\mathbf{z}}_{GSE}\right)\hat{\mathbf{z}}_{GSE}, \tag{9}$$

can be shown to correspond to GSE time (modulo 24 hr)

$$t_{GSE} = (12/\pi)\arccos\left(\mathbf{r}_{a\_xy}^T\hat{\mathbf{y}}_{GSE}/\left\|\mathbf{r}_{a\_xy}\right\|_2\right) \tag{10}$$

Apogee solar latitude at Phases 1a, 1b:

The solar latitude λ of the apogee vector, i.e. the perpendicular angle between it and the ecliptic, is given from

$$\cos(\pi/2 - \lambda) = \hat{\mathbf{r}}_a^T\hat{\mathbf{z}}_{GSE}, \tag{11}$$

or

$$\lambda = \arcsin\left(\cos\omega\sin\Omega\sin\varepsilon + \sin\omega\cos\Omega\cos i\sin\varepsilon - \sin\omega\sin i\cos\varepsilon\right). \tag{12}$$

Note that no quadrant ambiguity issues arise, as λ is defined to lie in the range [-90 deg, 90 deg].

Apogee-raising fuel usage

It is not at first obvious that the fuel usage for MMS apogee-raising is tied directly to the orientation of the orbit. This is a consequence of the fact that the MMS spacecraft are spinners, with long wire booms deployed, and therefore cannot readily be reoriented: their spin axis must therefore remain close to the ecliptic normal, the baseline attitude for science collection. Furthermore, each spacecraft has 8 radial thrusters, firing perpendicular to the spin axis, and 4 smaller axial thrusters, oriented along the axis. If a Delta-v must be applied in a direction that is far from either the spin axis or the spin plane, it must therefore be made up of a combination of the corresponding radial and axial components. In the worst case where the angle is 45 deg, a Triangle Inequality fuel penalty of around 41% will result. For the specific case of apogee-raising, each burn arc covers a wide range of the orbit around perigee, since the MMS thrusters are so small (4 lbf radial and 1 lbf axial). Consequently, if the perpendicular angle between the orbit plane and the spacecraft spin plane becomes large, significant Triangle Inequality penalties will occur: this could increase fuel usage, in the worst case, by something like 50 kg.

The obvious geometric proxy in this case is the perpendicular angle between the MMS spin planes and orbit plane, i.e. between the spin axis and the orbit normal. Since the spin axis is approximately aligned with the ecliptic normal, this angle is given as

$$\cos\gamma = \hat{\mathbf{h}}^T\hat{\mathbf{z}}_{GSE}; \tag{13}$$

from Eqs. (2) and (3), this can be written as

$$\gamma = \arccos\left(\cos\Omega\sin i\sin\varepsilon + \cos i\cos\varepsilon\right). \tag{14}$$

It will be shown that RAAN Ω varies, to a first approximation, linearly with time as a result of oblateness: this then leads (see Fig. 2) to a significant progression of γ over time. The key for good apogee-raising fuel consumption is to choose initial RAAN and AOP values so that, once RAAN has evolved to its Phase 2a value, γ is small enough that the spin axis and orbit normal vectors are "close".

Eclipse duration, Phase 2b

Excessive eclipses will occur during the critical phase of the mission, Phase 2b, if apogee (where the satellites are traveling fly the slowest) passes too deeply through the shadow cone of the Earth. This can be prevented by ensuring that apogee have a solar latitude large enough in magnitude that it misses the shadow region, or only passes through its edge. A condition (a lower limit) based on the apogee solar latitude λ can therefore be used to ensure that Phase 2b eclipses do not exceed the specified maximum duration. In fact, this lower limit on solar latitude must be applied for the entire low-speed region surrounding apogee: these latitudes are given by expressions very similar to that of Eq. (12), but involving the true anomaly of the boundary points also.

Neutral sheet dwell time

The Fairfield model (see Fig. 3) for the neutral sheet is given in terms of the GSM coordinate frame as

$$\delta z_{GSM} = \left\{ \left(H_0 + D \right) \sqrt{1 - \left(y_{GSM} / Y_0 \right)^2} - D \right\} \sin \chi \tag{15}$$

where $H_0 = 10.5 R_E$, $D = 14 R_E$, $Y_0 = 22.5 R_E$ and the angle χ is the geomagnetic latitude of the sub-solar point. MMS is deemed to be flying in the neutral sheet if its position vector has GSM z component within $\pm \pm 0.5 R_E$ of δz_{GSM} as determined from the Fairfield model.

Note that χ exhibits both seasonal (as a result of the angle of 23.4 deg between the ecliptic and the equator) and diurnal (as a result of the angle of approximately 11 deg between the Earth spin and dipole axes, leading to a daily "rocking" of the dipole) variations. Fig. 4 superimposes these variations and shows them in the GSE frame for the cases of three specific days, one (solid) with the Sun line 23.4 deg above the equator, one (dotted) with it lying in the equator, and one (dashed) with it 23.4 deg below. Clearly, in order for the spacecraft to spend a significant time within the neutral sheet, the range of apogee vectors in Phase 2b should be broadly aligned with these regions, i.e. not exceeding a GSE z component magnitude of roughly 5 R_E: this again reduces to a constraint on apogee solar latitude in Phase 2b. Contrary to the lower limit on solar latitudes that was derived for Phase 2b eclipses, however, this constraint is an upper limit. In fact, one of the main challenges in determining a viable MMS launch window is balancing the broadly conflicting eclipse and neutral sheet dwell time solar latitude constraints.

KEY ORBITAL PERTURBATIONS

Two orbital perturbations are significant for MMS: the oblateness of the Earth, and third-body gravitational attraction from the Sun and Moon. Other perturbations, for instance higher-order Earth gravitational harmonics, solar radiation pressure and the absolute orbital effects of the formation maneuvers used to control the relative positions of the spacecraft, must be taken into account when carrying out a high-fidelity simulation of the MMS orbital dynamics, as is done in the MMS ETE simulation code. However, for the purposes of a rapid scan of possible launch conditions, considering such small terms is not only not necessary, but positively unproductive: they would slow the computation unnecessarily. This is a manifestation of what might be termed the *Mosquito Principle*, by analogy with the design principles behind the British de Havilland Mosquito aircraft of World War 2[2]. In this approach, the launch window code began with an extremely simplified model (e.g. neglecting formation maintenance maneuvers and lunisolar effects, solar radiation pressure, higher-order Earth gravity harmonics, and assuming circular

[2] Over 7,000 of these flew in various roles: the key to its success was its great speed, which followed from its lightweight structure. This was achieved by a design process of successive improvement: in initial static testing, the rear wing spar failed at 88% of the design load [3]. This was then strengthened, the aircraft retested, the next component to fail strengthened, etc., leading to an efficient structure that met its 120% design load requirement.

orbits for the Earth about the Sun and for the Moon about the Earth); this was tested and aspects that were found wanting (e.g. the neglected lunisolar effects and the orbital eccentricity of Earth) corrected, until good agreement with ETE spot test results was obtained. The result of this approach is a model that is accurate enough for launch window work, but not so excessively high-fidelity that it is computationally onerous.

Details on the key orbital perturbations for MMS will now be given.

Oblateness Effects

The dominant orbital effects of oblateness are the secular rates that it produces in RAAN and AOP: these averaged rates are given [4] as

$$\dot{\bar{\Omega}} = -1.5nJ_2(R_E/p)^2\cos i \tag{16}$$

and

$$\dot{\bar{\omega}} = 3.75nJ_2(R_E/p)^2[0.8-\sin^2 i]\,, \tag{17}$$

where the mean motion $n=\sqrt{\mu_{Earth}/a^3}$, and the dimensionless $J_2 = 1.0827\times10^{-3}$. These rates depend only on the orbital elements *a*, *e* and *i*, and are decoupled: changes in RAAN do not affect the rate of change of AOP, and *vice versa*.

The changes in RAAN and AOP that are produced by Eqs. (16) and (17) over a (30-day) month for MMS are given in Table 1. The reduced rates in Phase 2b that follow from its reduced mean motion (and essentially unchanged *p* value) are evident. An important point to observe is how large oblateness effects are for MMS: over the roughly 2.5-year mission, they cause a RAAN decrease of about 80 deg, and an AOP increase of around 130 deg.

Table 1. Monthly oblateness effects for MMS mission phases.

Change per (30-day) month	Phase 1	Phase 2b
RAAN	-3.255	5.299
AOP	-1.057	1.720

Lunisolar Effects

It is not the absolute gravitational accelerations that the Sun and Moon exert on the MMS spacecraft that are important in a study of orbital perturbations, but rather the differences between the third-body accelerations that act on the spacecraft and the corresponding accelerations that act on the Earth itself. It is these differential accelerations that will tend to cause the spacecraft orbit to diverge from a Keplerian one. Taking the solar case first, this differential acceleration can be written as

$$\mathbf{a}_{Sun/sat} = \left(\frac{\mu_{Sun}}{r_{Sun/sat}^3}\right)\mathbf{r}_{Sun/sat} - \left(\frac{\mu_{Sun}}{r_{Sun}^3}\right)\mathbf{r}_{Sun}\,, \tag{18}$$

where $\mathbf{r}_{Sun}$ is the Earth-to-Sun vector and $\mathbf{r}_{Sun/sat}$ that from satellite to Sun; the scalars $r_{Sun/sat}$ and r_{Sun} are the lengths of these vectors. Writing

$$\mathbf{r}_{Sun/sat} = \mathbf{r}_{Sun} - \mathbf{r}_{sat}\,, \tag{19}$$

with $\mathbf{r}_{sat}$ the position vector of the satellite relative to the Earth, an approximation to the differential acceleration, valid to first order in the small quantity r_{sat}/r_{Sun}, can be shown to be

$$\mathbf{a}_{Sun/sat} \approx \left(\frac{\mu_{Sun}}{r_{Sun}^3}\right)\left\{3\left(\frac{r_{sat}}{r_{Sun}}\right)\cos\alpha\mathbf{r}_{Sun} - \mathbf{r}_{sat}\right\}, \tag{20}$$

where α is the angle between $\mathbf{r}_{Sun}$ and $\mathbf{r}_{sat}$, i.e. $\mathbf{r}_{Sun}^T\mathbf{r}_{sat} = r_{Sun}r_{sat}\cos\alpha$. In terms of unit vectors, this can in turn be rewritten as

$$\mathbf{a}_{Sun/sat} \approx \left(\frac{\mu_{Sun}}{r_{Sun}^3} \right) r_{sat} \left\{ 3\cos\alpha \hat{\mathbf{r}}_{Sun} - \hat{\mathbf{r}}_{sat} \right\} . \tag{21}$$

Note that this relative acceleration is basically proportional to the distance r_{sat} between Earth and satellite, and so tends to be largest in the region around apogee, although the relative directions of Sun and satellite from Earth are important also.

The differential lunar perturbation can be dealt with in analogous manner, giving an equivalent first-order approximation. Since the ratio r_{sat}/r_{Moon} is not far smaller than unity for MMS (especially for Phase 2b), it at first appears that a second-order approximation will be required. However, the approach taken in the current work averages the differential lunar effects over a complete lunar orbit: this allows relatively long step sizes (e.g. 10 days) to be used in the launch window analyzer without concerns over the exact phasing between Moon and satellite. It also obviates the need for detailed lunar ephemeris data: only the lunar orbit normal need be characterized accurately. (The penalty of this lunar-averaging approach is the loss of lunar short-period oscillations in the orbital elements: these are small fluctuations, with periods of roughly 14 days, and are not key to study of the MMS launch window.) When this averaging is carried out, and assuming that the lunar orbit is perfectly circular (see the Mosquito Principle), the second-order terms cancel, returning to a first-order net approximation.

Lunisolar effects on RAAN and AOP are not as large as those produced by oblateness: typical net changes over the course of the mission are 10-20 deg. However, these perturbations differ in that they vary considerably as a function of launch date and initial orbit orientation. Furthermore, lunisolar effects (not only in RAAN and AOP, but also in elements such as inclination and eccentricity that are not affected secularly by oblateness), are highly coupled. These facts make the study of lunisolar perturbations for MMS much more challenging than quantifying the oblateness effects.

VOP EQUATIONS AND ORBIT AVERAGING

The effect of the differential lunisolar accelerations on the MMS orbit can be studied efficiently using the *Variation of Parameters* equations [5]: these describe the changes in the orbital elements that are produced by small perturbation accelerations as a function of where on the orbit they act. The Gaussian form of the first five of these equations can be written in terms of the perturbation acceleration vector when this is expressed as its components in the satellite local radial/tangential/orbit normal rotating frame, termed the RSW frame [6]: the *R*-axis is directly radially outwards, *W* along the orbit angular momentum, and *S* along the forward tangent, completing a right-handed triad). The resulting VOP equations are then

$$\dot{a} = \frac{2}{n\sqrt{1-e^2}} \left\{ e\sin\nu a_R + (1+e\cos\nu) a_S \right\} , \tag{22}$$

$$\dot{e} = \frac{\sqrt{1-e^2}}{na} \left\{ \sin\nu a_R + \frac{(e+2\cos\nu+e\cos^2\nu)}{(1+e\cos\nu)} a_S \right\} , \tag{23}$$

$$\dot{i} = \frac{r\cos(\omega+\nu)}{na^2\sqrt{1-e^2}} a_W , \tag{24}$$

$$\dot{\Omega} = \frac{r\sin(\omega+\nu)}{na^2\sqrt{1-e^2}\sin i} a_W \tag{25}$$

and

$$\dot{\omega} = \frac{\sqrt{1-e^2}}{nae} \left\{ -\cos\nu a_R + \sin\nu \frac{(2+e\cos\nu)}{(1+e\cos\nu)} a_S - \frac{e\cot i \sin(\omega+\nu)}{(1+e\cos\nu)} a_W \right\} . \tag{26}$$

A corresponding equation also exists for the mean anomaly at epoch, M_0, serving to describe how the phasing of the satellite is affected by the perturbations. However, the precise phasing of the MMS spacecraft need not be characterized in order to solve the launch window problem using the current approximation methods; this sixth VOP equation is therefore not required.

The right-hand sides of Eqs. (22-26) involve the instantaneous values of the orbital elements, and are exact expressions. However, if the applied perturbations are small, the changes in the elements over a single MMS orbit will also be relatively small: this permits the simplification of holding the values constant while evaluating the VOP expressions over each MMS rev. The resulting *orbit-averaged* values for the changes in each element are approximations, but are close to the true values for small perturbations, as is the case here. It should be noted that the secular oblateness-induced rates of Eqs. (16) and (17) were themselves derived [4] using orbit-averaging of the VOP equations, with the applied perturbation acceleration components in this case being those produced by the J_2 term in the Earth gravity harmonic expansion.

As an example, the orbit-averaged change in SMA will now be derived: this will also serve to show a detail that is involved. This is the fact that Eq. (22) gives the time rate of change of SMA in terms of true anomaly, not time; integrating to find Δa_{rev} therefore requires the change of variables

$$\Delta a_{rev} = \int_0^T \dot{a}\, dt = \int_0^{2\pi} \dot{a}(\nu) \frac{dt}{d\nu} d\nu = \int_0^{2\pi} \left(\dot{a}(\nu) / \dot{\nu} \right) d\nu \,. \tag{27}$$

But the angular momentum of the MMS orbit can be expressed in two forms, as

$$h = \dot{\nu} r^2 = \sqrt{\mu_{Earth} p} \,. \tag{28}$$

This then implies that

$$\dot{\nu} = \frac{h}{r^2} = \frac{\sqrt{\mu_{Earth} p}}{p^2} (1 + e\cos\nu)^2 = \sqrt{\frac{\mu_{Earth}}{p^3}} (1 + e\cos\nu)^2 \,. \tag{29}$$

Combining this with Eqs. (22) and (27) then gives

$$\begin{aligned} \Delta a_{rev} &= \int_0^{2\pi} \sqrt{\frac{p^3}{\mu_{Earth}}} \frac{\dot{a}(\nu)}{(1 + e\cos\nu)^2} d\nu \\ &= \int_0^{2\pi} \sqrt{\frac{a^3 (1-e^2)^3}{\mu_{Earth}}} \frac{2}{n\sqrt{1-e^2}} \left\{ \frac{e \sin\nu a_R}{(1 + e\cos\nu)^2} + \frac{a_S}{(1 + e\cos\nu)} \right\} d\nu \\ &= \int_0^{2\pi} \frac{2(1-e^2)}{n} \sqrt{\frac{a^3}{\mu_{Earth}}} \left\{ \frac{e \sin\nu a_R}{(1 + e\cos\nu)^2} + \frac{a_S}{(1 + e\cos\nu)} \right\} d\nu \\ &= \int_0^{2\pi} 2(1-e^2) \left(\frac{a^3}{\mu_{Earth}} \right) \left\{ \frac{e \sin\nu a_R}{(1 + e\cos\nu)^2} + \frac{a_S}{(1 + e\cos\nu)} \right\} d\nu. \end{aligned} \tag{30}$$

Note the terms $(1 + e\cos\nu)$ and $(1 + e\cos\nu)^2$ in the denominator. In fact, denominator terms of the form $(1 + e\cos\nu)^l$, l = 2–4 are found in the VOP orbit-averaged lunisolar element changes: as well as those already seen, other terms of this form arise from the VOP equations themselves (Eqs. (23) and (26)), and others from the satellite radius $r_{sat} = p/(1 + e\cos\nu)$ that multiplies the lunisolar acceleration of Eq. (21).

The resulting orbit-averaged VOP expressions for the effects of lunisolar perturbations on the MMS orbit can be summarized as follows. Note that they are considerably more complicated than were the oblateness effects; specifically, more elements are affected, and their changes are coupled, either directly (the equation for the change of one quantity is written in terms of the other) or indirectly (the lunisolar acceleration components themselves depend upon the other element).

Solar perturbations

$$\Delta i_{rev_S} = -\tfrac{1}{2} e \kappa_{Sun} \left(\hat{\mathbf{r}}_{Sun}^T \hat{\mathbf{h}} \right) \begin{Bmatrix} \cos\omega \cos\alpha_{apo_{Sun}} \left[I(1,4) + I(\cos 2\nu, 4) \right] \ldots \\ \ldots + \sin\omega Q_{Sun} \left[-I(1,4) + I(\cos 2\nu, 4) \right] \end{Bmatrix}, , \tag{31}$$

$$\Delta\Omega_{rev_S} = -\tfrac{1}{2} e \kappa_{Sun} \operatorname{cosec} i \left(\hat{\mathbf{r}}_{Sun}^T \hat{\mathbf{h}} \right) \begin{Bmatrix} \sin\omega \cos\alpha_{apo_{Sun}} \left[I(1,4) + I(\cos 2\nu, 4) \right] \ldots \\ \ldots + \cos\omega Q_{Sun} \left[I(1,4) - I(\cos 2\nu, 4) \right] \end{Bmatrix}, \tag{32}$$

and $\Delta\omega_{rev_S} = \Delta\omega_{rev_{S\_R}} + \Delta\omega_{rev_{S\_S}} + \Delta\omega_{rev_{S\_W}}$, where the three terms

$$\Delta\omega_{rev_{S\_R}} = -\tfrac{1}{2}\kappa_{Sun}\begin{Bmatrix}\cos^2\alpha_{apo_{Sun}}\left[I(\cos\nu\cos 2\nu,3)+I(\cos\nu,3)\right]\ldots\\ \ldots+\cos\omega Q_{Sun}\left[-I(\cos\nu\cos 2\nu,3)+I(\cos\nu,3)\right]\ldots\\ \ldots-\tfrac{2}{3}I(\cos\nu,3)\end{Bmatrix}, \tag{33}$$

$$\Delta\omega_{rev_{S\_S}} = -\kappa_{Sun}\left[\cos^2\alpha_{apo_{Sun}} - Q_{Sun}^2\right]I(\sin^2\nu\cos\nu(2+e\cos\nu),4) \tag{34}$$

and

$$\Delta\omega_{rev_{S\_W}} = -\cos i\,\Delta\Omega_{rev_S}\,, \tag{35}$$

where

$$\kappa_{Sun} = 3\left(\frac{\mu_{Sun}}{\mu_{Earth}}\right)\left(\frac{a}{r_{Sun}}\right)^3\frac{\left(1-e^2\right)^3}{e} \tag{36}$$

and the quantities Q_{Sun} and $\cos\alpha_{apo_{Sun}}$ are defined by the relative geometry of the MMS orbit and the Earth-Sun line. In addition, the integrals $\{I(f,l)\}$ are defined as

$$I(f,l) \equiv \int_0^{2\pi}\frac{f(\nu)d\nu}{(1+e\cos\nu)^l}\,. \tag{37}$$

Lunar perturbations

These are essentially of the same form as Eqs. (31-35), with κ_{Sun} replaced by the exactly analogous κ_{Moon}, the terms Q_{Sun} and $\cos\alpha_{apo_{Sun}}$ replaced by quantities that now depend on the relative geometry of the MMS and lunar orbits, and with an overall multiplier of one half reflecting the fact that the effects are averaged over a lunar orbit.

Combined lunisolar perturbations

Finally, an important effect of the combined lunisolar perturbations is that they can cause significant changes in the radius of perigee: this can, in extreme cases, lead to unplanned reentry, or can require MMS to carry out a perigee reboost maneuver, at the expense of considerable fuel. Using the same VOP orbit-averaging approach, these changes in perigee radius (essentially caused by changes in eccentricity) as given as

$$\begin{aligned}\Delta r_{p\_rev_{SM}} = {} & ae\left\{K_{Sun}Q_{Sun}\cos\alpha_{apo\_Sun} + K_{Moon}C_M\right\}\ldots\\ & \ldots\times\left\{2I(\cos 2\nu,2) - I(\cos 2\nu(e+2\cos\nu+e\cos^2\nu),4) + eI(\sin\nu\sin 2\nu,3)\right\},\end{aligned} \tag{38}$$

where the quantity C_M is defined by the MMS/lunar orbits relative geometry.

MAXIMIZING COMPUTATIONAL EFFICIENCY

The orbit-averaged VOP equation method for the determination of the effects of the lunisolar and oblateness perturbations on the MMS orbit, together with the use of geometric proxies for evaluation of the orbital constraints, has been implemented in Matlab for use as a launch window analyzer. This program, termed SWM76, has also been translated into Python, in order to take advantage of the improved graphics capabilities that this language provides. SWM76 does not require any Matlab specialized toolboxes: it only uses basic functions such as sin, cos, sqrt etc. As has already been noted, steps were taken to ensure that this analyzer was relatively fast to run: these include the use of the orbit-averaged VOP equations, the use of geometric proxies, and averaging lunar effects over an entire lunar orbit, so allowing time steps of on the order of 10 days.

In addition, since Matlab can run a computation over an entire matrix faster than if it were to perform a double loop over the rows and columns of this matrix, performing the computation on each individual

element in turn, the matrix approach is taken in SWM76. In particular, if a complete scan over 360 deg of RAAN and 360 deg of AOP, in steps of 2 deg, were to be performed for a given launch day, matrices of orbital element initial conditions,

$$\Omega_{0\_mat} = \begin{pmatrix} 0 & 2 & \cdots & 360 \\ \vdots & \vdots & \ddots & \vdots \\ 0 & 2 & \cdots & 360 \\ 0 & 2 & \cdots & 360 \end{pmatrix} \text{deg}, \tag{39}$$

$$\omega_{0\_mat} = \begin{pmatrix} 360 & 360 & \cdots & 360 \\ \vdots & \vdots & \ddots & \vdots \\ 2 & 2 & \cdots & 2 \\ 0 & 0 & \cdots & 0 \end{pmatrix} \text{deg} \tag{40}$$

and

$$i_{0\_mat} = \begin{pmatrix} 28.5 & 28.5 & \cdots & 28.5 \\ \vdots & \vdots & \ddots & \vdots \\ 28.5 & 28.5 & \cdots & 28.5 \\ 28.5 & 28.5 & \cdots & 28.5 \end{pmatrix} \text{deg} \tag{41}$$

are first set up. Performing all operations of the form of Eqs. (16-17) and (31-36) on these matrices then evaluates the orbital perturbations for all of these initial condition cases simultaneously. (Given the coupling between the lunisolar perturbation results for the various elements, each of these initial conditions will indeed generally lead to unique results.)

One final step that is taken to increase computational efficiency involves the calculation of the integrals of Eq. (37). These are strong functions of eccentricity, as is evidenced by Table 2. This table shows the values of the eight integrals used here for the MMS Phase 1 (eccentricity 0.8182) and Phase 2b (eccentricity 0.9084) orbits. Since lunisolar effects can affect eccentricity, the values used for these integral be used must be corrected accordingly. Instead of computing them directly by numerical integration, which would be excessively computationally expensive, SWM76 evaluates them using spline approximations.

Table 2. Integral values for MMS mission phases.

Integral	Phase 1	Phase 2b
$I(\cos 2\nu, 2)$	19.18	64.77
$I(\cos\nu, 3)$	-122.73	-670.04
$I(\cos\nu\cos 2\nu, 3)$	-99.28	-598.74
$I(\sin\nu\sin 2\nu, 3)$	-23.44	-71.30
$I(1, 4)$	606.24	6294.64
$I(\cos 2\nu, 4)$	506.24	5802.90
$I(\sin^2\nu\cos\nu(2+e\cos\nu), 4)$	-52.63	-259.00
$I(\cos 2\nu(e+2\cos\nu+e\cos^2\nu), 4)$	-181.10	-1045.43

The end result of this emphasis on computational speed is that SWM76 can evaluate the 32,400 initial conditions involved in performing a complete scan, at 2 deg granularity, over (RAAN, AOP) space for a given launch date in less than 10 s on a typical modern laptop. For comparison, a previous MMS launch window scan program, based on point-by-point orbit propagation and direct evaluation of eclipses, etc., required around 15 min to carry out a coarser scan of a relatively small portion of the (RAAN, AOP) space. Also, the high-fidelity MMS ETE simulation code, which carries out a far more detailed evaluation than does SWM76, including all formation maintenance and resize maneuvers, the effects of maneuver execution and navigation errors, and the details of a sophisticated model of the propulsion system, requires

on the order of 6-8 hours to complete a single mission simulation. At this rate, scanning over 32,400 cases on a single processor would require 22-30 years.

RESULTS AND IMPLICATIONS FOR CONSTRAINT RELAXATION

The way in which SWM76 is used is as a pathfinder for the ETE simulation code (rather as the Mosquito was used by the Pathfinders to mark the target for the main bomber force), providing launch values for RAAN and AOP that are expected to satisfy the orbital requirements for launch on the given date. These values are then used to initialize (i.e. seed) the ETE code, which tests whether all orbital requirements are actually satisfied. The ETE can also be used to carry out Monte Carlo studies of the effects of maneuver and navigation errors. The ETE results are what are used to definitively decide whether a given launch date and orbit are acceptable; however, given the length of time required to run this simulation, it would not be practical to use it to test a large set of initial conditions in order to identify a launch window. SWM76 and the ETE code therefore complement each other well. It should also be noted that agreement between their results has been found, during quite an extensive testing program, to be very good: Figs. 5 shows the evolution of RAAN as computed in the ETE code (solid curve) with spot checks of the results of SWM76 (green points) for one particular Aug. 29, 2014 launch case. The close agreement between the two algorithms can clearly be seen. (The results for RAAN and inclination for this test case are similarly close.) For interest, the results that are obtained if only J_2 effects, but not the lunisolar terms, are included are marked as red points: it can be seen that J_2 produces the bulk of the change in RAAN, but by no means its entirety.

As already discussed, the results output by SWM76 are plots of (RAAN, AOP) space for a given launch date of the form shown by Figs. 6-9. In each case, the boundaries of the regions over which each of the constraints is satisfied are denoted by curves of different colors; the colors, and the ways in which the curves are to be interpreted in order to satisfy the constraints, are indicated in the figure title. Fig. 6 is for the case of a launch on Oct. 15, 2014: the unshaded lozenge is the intersection of all of the constraint satisfaction regions, and is therefore the available launch window. Fig. 7 is the corresponding plot for a launch on Aug. 29, 2014: it can be seen that no launch window exists for the baseline orbital requirements. However, after consultation with both the MMS engineering and science communities, relaxations were investigated to the early eclipse, Phase 1a and 1b solar latitude, Phase 1 GSE start time and Phase 2b eclipse limits: with these relaxations, the launch window indicated in Fig. 8 was produced for the same launch date. If, in addition, a small apogee-raise maneuver of 1.5 R_E were carried out during Phase 1x as a trial for the later Phase 2a maneuvers, a further widening of the window lozenge was obtained, as shown in Fig. 9. This improvement can be explained as follows: raising apogee decreases the effects of oblateness on the orbit. This therefore makes the orbit "appear" to have been in existence for a shorter time, i.e. launch appears to have been later, and so closer to the more favorable Oct.-Nov. period.

Finally, Fig. 10 illustrates the range of perigee altitude variation that can be caused by lunisolar effects: the plot shows the minimum perigee altitude reached at any point in the mission, as a function of launch RAAN and AOP, for launch on Oct. 15, 2014. Negative altitudes are seen for some launch conditions, but fortunately (see Fig. 6) not in the vicinity of the Oct. 15 launch window. This information is useful for predicting how many perigee maintenance maneuvers MMS will be required to carry out: since each of these consumes around 30 kg of fuel out of the 410 kg MMS total, this question is of considerable practical importance.

CONCLUSIONS

The orbit-averaged VOP equation approach to evaluating the effects of orbital perturbations for the MMS mission has proved to be quite accurate, and very efficient computationally. This efficiency allows evaluation of the evolution of the launch window over the entire year, so enabling parametric studies to be carried out: one example considered to date is that of changing the apogee radius of the orbit. In addition, the graphical results that are produced provide great insight into how severely each orbital constraint affects the extent of the window, and therefore how productive it is likely to be, in terms of opening up a tight

window, to either relax or eliminate a given requirement. This semi-analytical approach to launch window analysis could also productively be applied to many other missions.

ACKNOWLEDGEMENTS

The author wishes to thank Conrad Schiff (for extensive discussions and encouragement, and for implementing the integral spline models), Edwin Dove (for comprehensive ETE testing and evaluation of SWM76) and Jason Tichy (for implementing the Python version of SWM76).

REFERENCES

[1] S. Curtis, *The Magnetospheric Multiscale Mission: Resolving Fundamental Processes in Space Plasmas*, NASA/TM-2000-209883, Dec. 1999.

[2] D.H. Fairfield, "A Statistical Determination of the Shape and Position of the Geomagnetic Neutral Sheet", *J. Geophysical Research*, Vol. 85, No. A2, pp. 775-780, Feb. 1980.

[3] J.E. Gordon, *Structures – Or Why Things Don't Fall Down*, Penguin Book Ltd., 1978.

[4] J.E. Prussing and B.A. Conway, *Orbital Mechanics*, Oxford University Press, 1993.

[5] R.R. Bate, D.D. Mueller and J.E. White, *Fundamentals of Astrodynamics*, Dover Publications, Inc., 1971.

[6] D.A. Vallado, *Fundamentals of Astrodynamics and Applications*, Microcosm Press/Springer Verlag, 2007 (3rd edition).

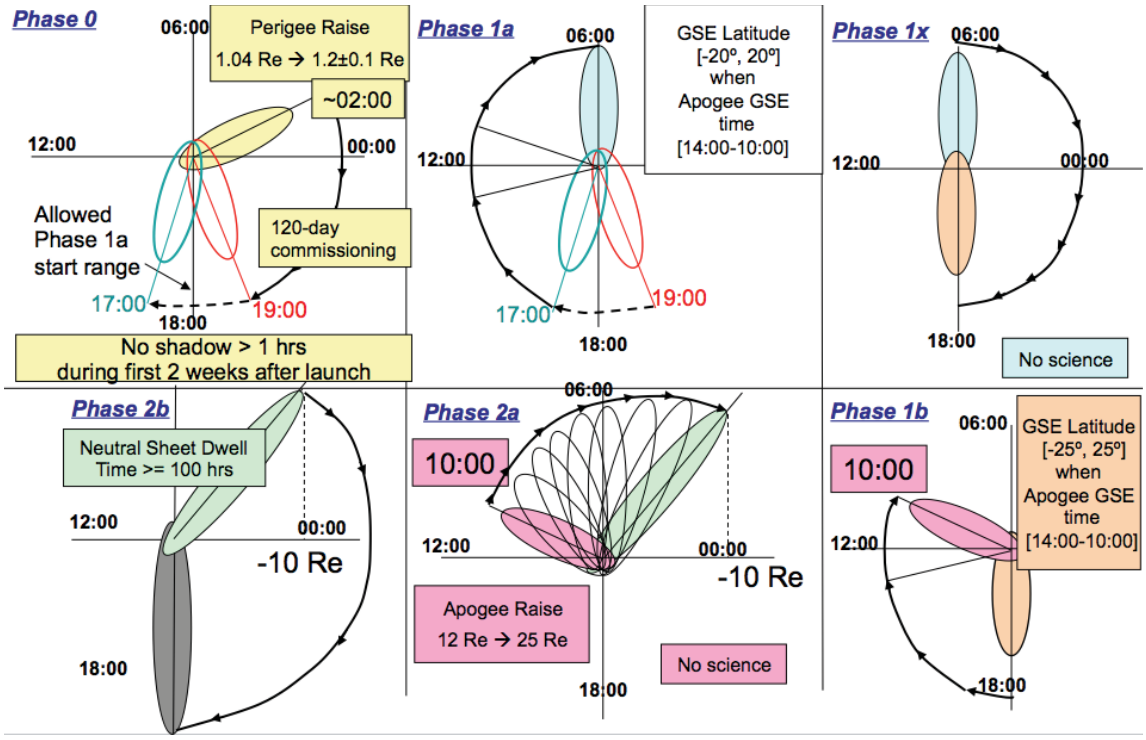

Figure 1. MMS Mission Phases (Clockwise from Top Left).

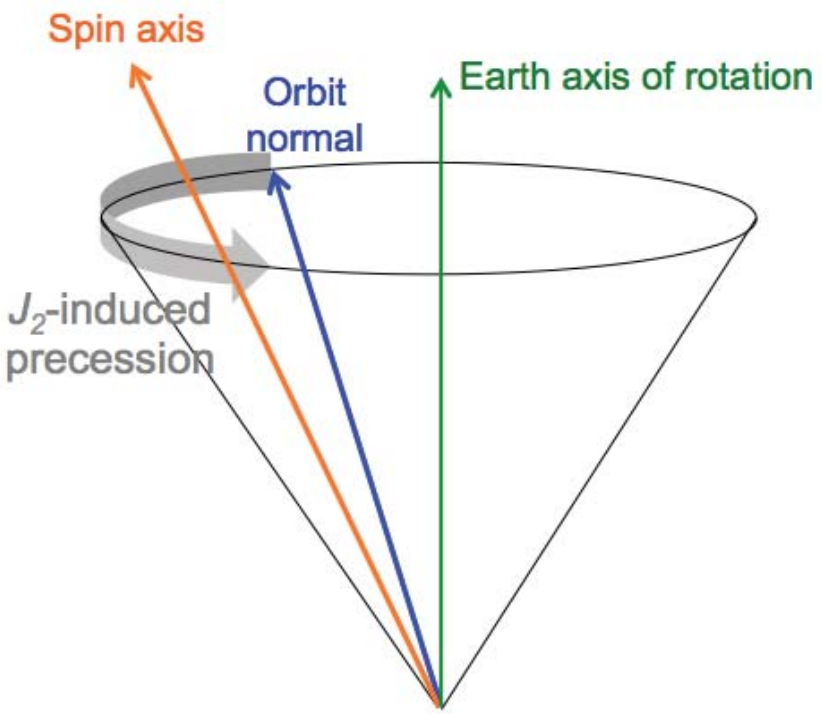

Figure 2. Evolution of Orbit Normal under J_2.

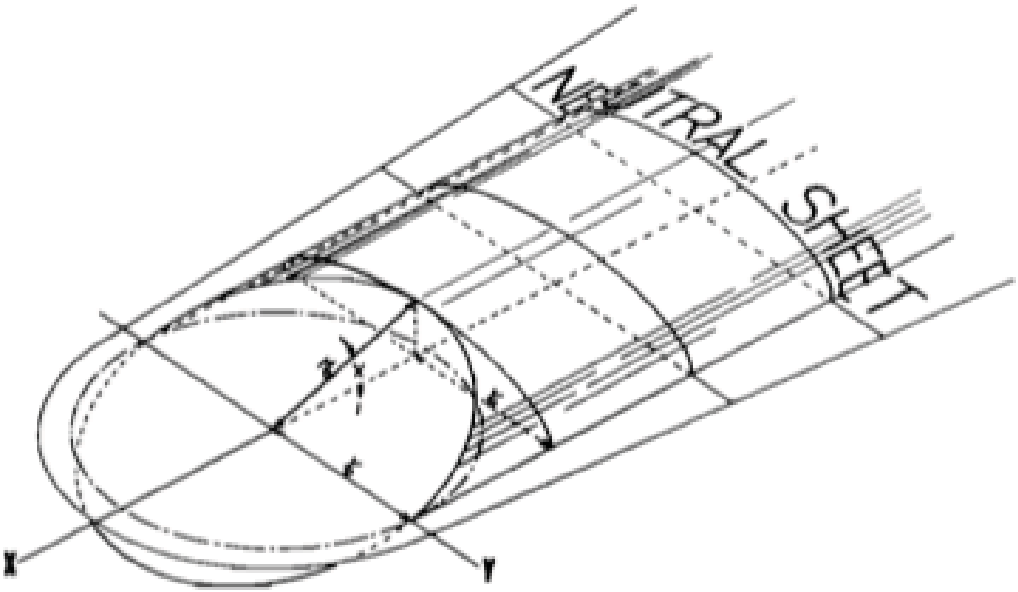

Figure 3. Fairfield Neutral Sheet Model.

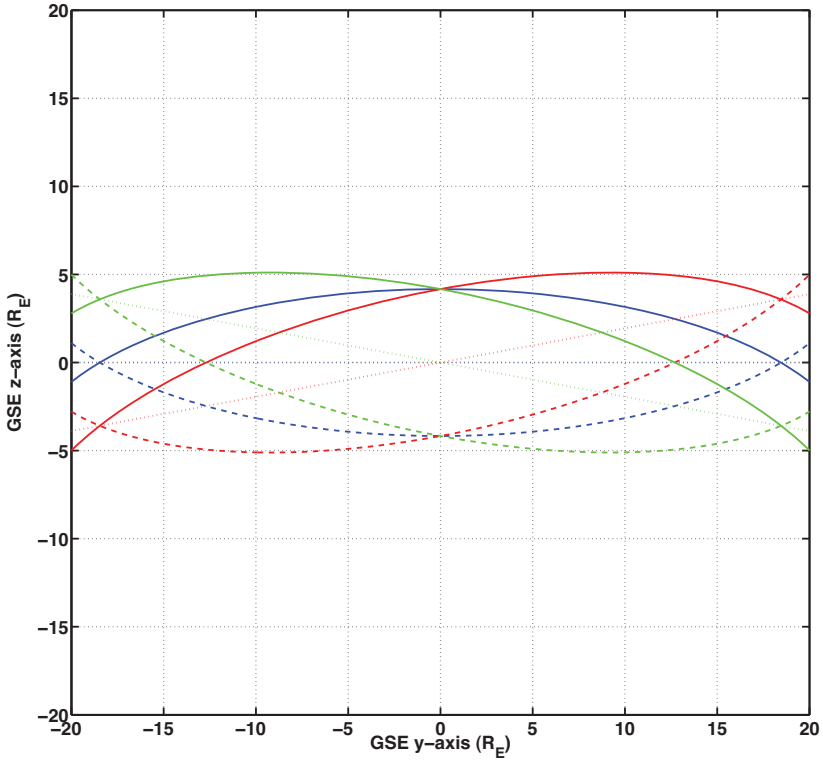

Figure 4. Diurnal Dipole Rocking Effects on Fairfield Model.

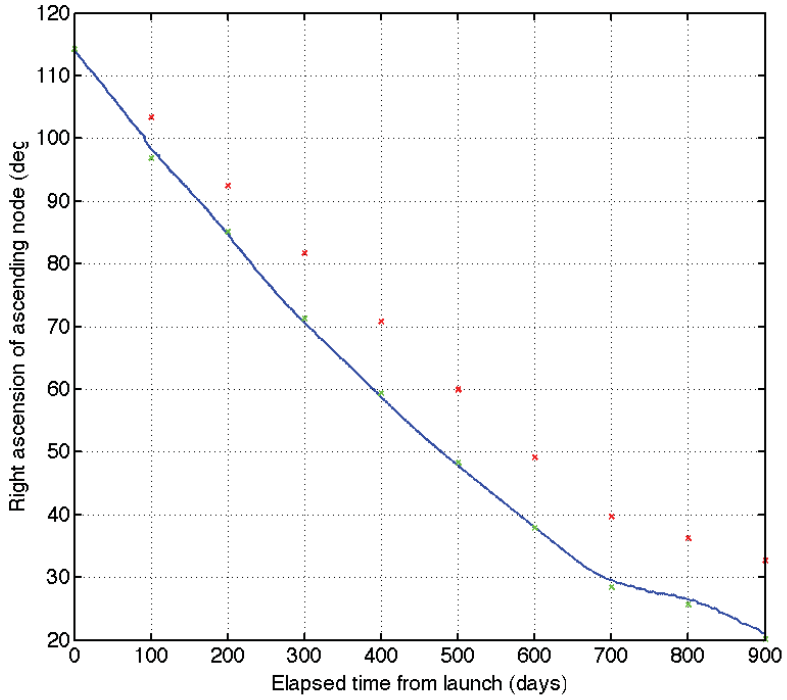

Figure 5. Evolution of RAAN, ETE (Solid) and SWM76 (Green Points).

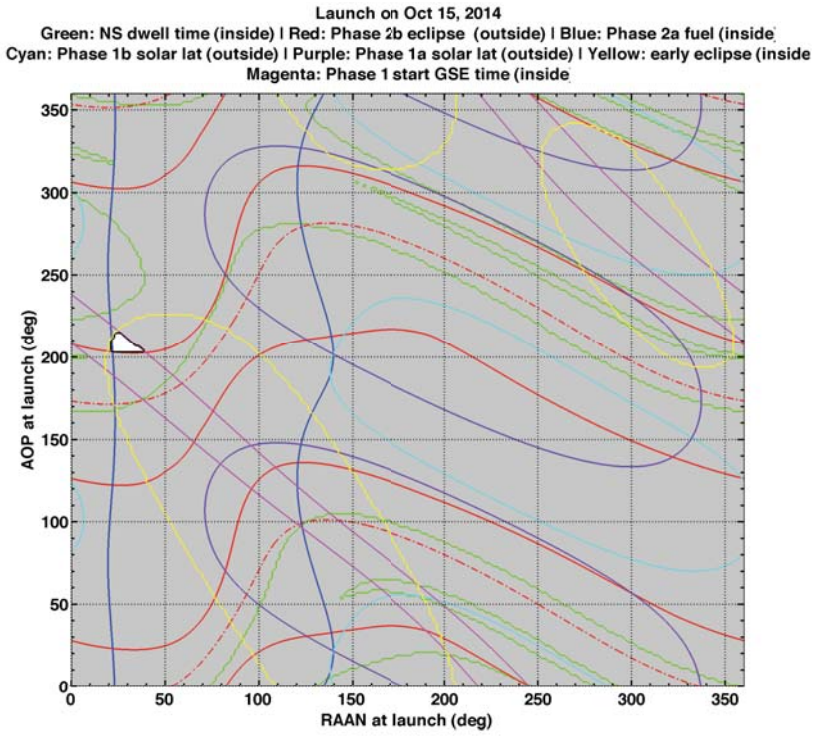

Figure 6. Launch Window Scan, Oct. 15, 2014 Launch.

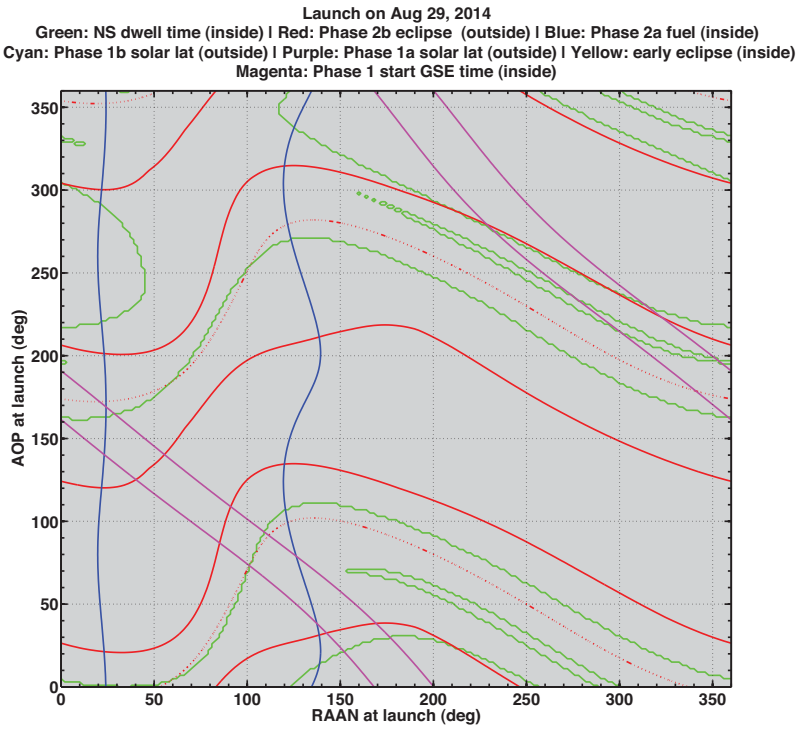

Figure 7. Launch Window Scan, Aug. 29, 2014 Launch, Baseline Constraints.

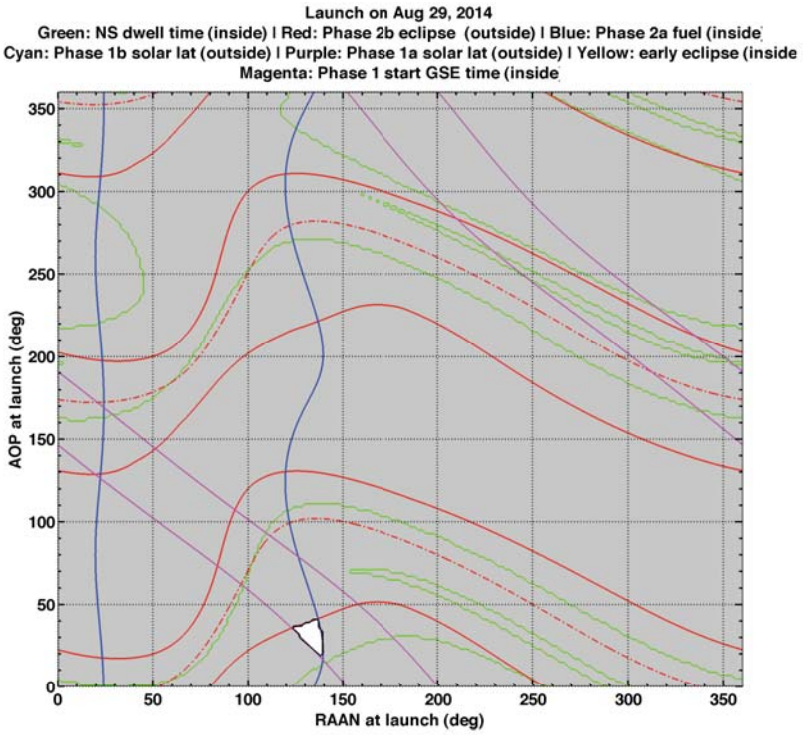

Figure 8. Launch Window Scan, Aug. 29, 2014 Launch, Relaxed Constraints.

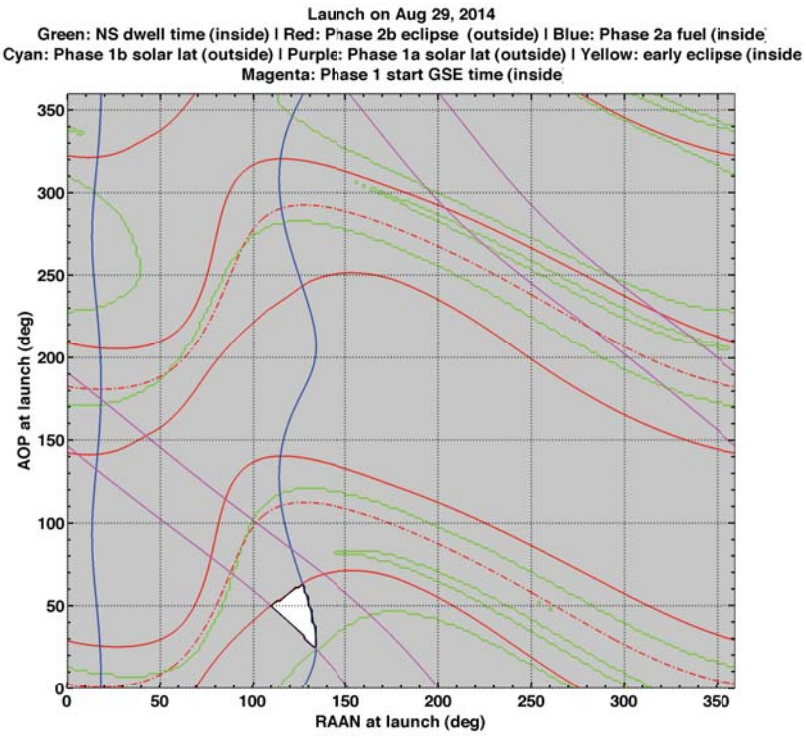

Figure 9. Launch Window Scan, Aug. 29, 2014 Launch, Phase 1x Apogee-Raise.

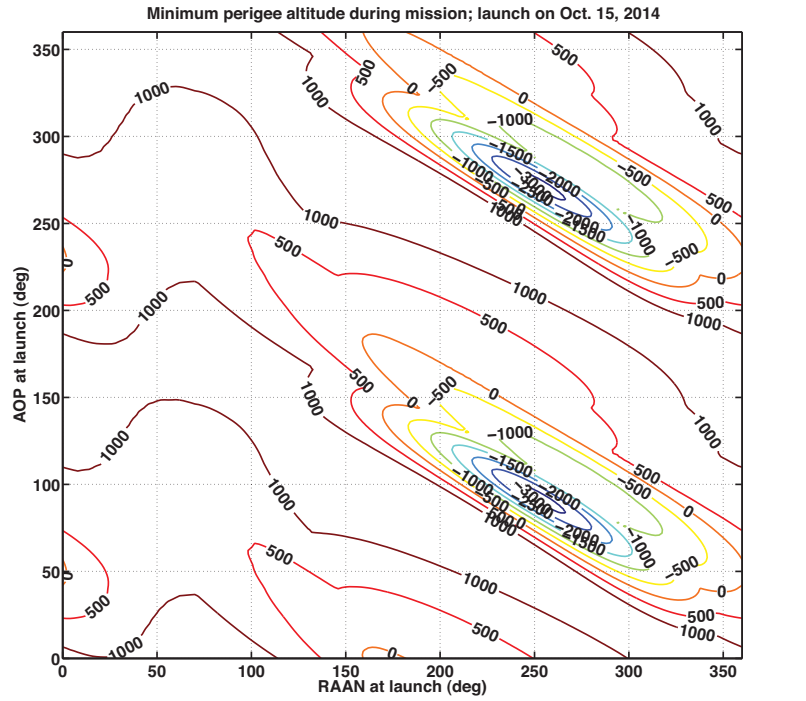

Figure 10. Minimum Perigee Altitude during Mission, Oct. 15, 2014 Launch.